

On the Feasibility of Detecting Satellites of Extrasolar Planets via Microlensing

Cheongho Han

Department of Physics, Chungbuk National University, Chongju 361-763, Korea

E-mails: `cheongho@astroph.chungbuk.ac.kr`

Wonyong Han

Korea Astronomy Observatory, Taejon 305-348, Korea

`whan@kao.re.kr`

ABSTRACT

Although many methods of detecting extra-solar planets have been proposed and successful implementation of some of these methods enabled a rapidly increasing number of exoplanet detections, little has been discussed about the method of detecting satellites around exoplanets. In this paper, we test the feasibility of detecting satellites of exoplanets via microlensing. For this purpose, we investigate the effect of satellites in the magnification pattern near the region of the planet-induced perturbations by performing realistic simulations of Galactic bulge microlensing events. From this investigation, we find that although satellites can often cause alterations of magnification patterns, detecting satellite signals in lensing light curves will be very difficult because the signals are seriously smeared out by the severe finite source effect even for events involved with source stars with small angular radii.

Subject headings: gravitational lensing – planets and satellites: general

1. Introduction

Various methods have been proposed to search for extrasolar planets (exoplanets). These methods include the pulsar timing analysis, direct imaging, accurate measurement of astrometric displacements, radial velocity measurement, planetary transit, and gravitational microlensing [see the review of Perryman (2000)]. Since the first detection of an exoplanet around the pulsar PSR 1257+12 (Wolszcan & Frail 1992), nearly 100 exoplanets have been identified (<http://exoplanets.org>), mostly by the radial velocity method (Mayor & Queloz 1995).

However, little has been discussed about the method of detecting satellites around exoplanets. This is mainly because it is thought to be too premature to detect satellites given the difficulties of detecting exoplanets. Currently, the only promis-

ing technique proposed to detect satellites is the transit method, where satellites are detected either by direct satellite transit or through perturbations in the transit timing of the satellite-hosting planet (Sartoretti & Schneider 1999).

In this paper, we investigate the feasibility of detecting satellites of exoplanets via microlensing. Detection of a low-mass companion by using microlensing is possible because the companion can induce noticeable anomalies in the resulting lensing light curves (Mao & Paczyński 1991; Gould & Loeb 1992). The microlensing method has an important advantage in detecting very low-mass companions over other methods because the strength of the companion's signal depends weakly on the companion/primary mass ratio although the duration of the signal becomes shorter with the decrease of the mass ratio. Then, if lensing events are monitored with a high enough frequency, it

may be possible to detect not only planets but also their satellites. Such a frequent lensing monitoring program in space was recently proposed by Bennett (2000).

The paper is organized as follows. In § 2, we describe the microlensing basics of multiple-lens systems. In § 3, we investigate the feasibility of satellite detections by carrying out realistic simulations of Galactic bulge microlensing events caused by an example lens system having a planet and a satellite. We summarize the results and conclude in § 4.

2. Multiple-lens Systems

To describe the lensing behaviors of events caused by a lens system composed of a primary with a planet and subordinate satellites, it is required to have the formalism of multiple-lens systems. If a source located at $\mathbf{r}_S(\xi, \eta)$ on the projected plane of the sky is lensed by a lens system composed of N -point masses, where the individual components' masses and locations are m_i and $\mathbf{r}_{L,i}$, the positions of the resulting images, \mathbf{r}_I , are obtained by solving the lens equation, which is expressed by

$$\mathbf{r}_S = \mathbf{r}_I - \theta_E^2 \sum_{i=1}^N \frac{m_i}{m} \frac{\mathbf{r}_I - \mathbf{r}_{L,i}}{|\mathbf{r}_I - \mathbf{r}_{L,i}|^2}. \quad (1)$$

Here θ_E represents the angular Einstein ring radius, which is related to the total mass of the lens system, $m = \sum_i^N m_i$, and the distances to the lens, D_{OL} , and the source, D_{OS} , by

$$\theta_E = \sqrt{\frac{4Gm}{c^2}} \left(\frac{1}{D_{OL}} - \frac{1}{D_{OS}} \right)^{1/2}. \quad (2)$$

The lensing process conserves the surface brightness of the source. Then the magnification of each image equals to the surface area ratio between the image and the unmagnified source and mathematically its value corresponds to the inverse of the Jacobian of the lens equation evaluated at the image position $\mathbf{r}_{I,j}$, i.e.

$$A_j = \left(\frac{1}{|\det J|} \right)_{\mathbf{r}_I=\mathbf{r}_{I,j}}; \quad \det J = \left| \frac{\partial \mathbf{r}_S}{\partial \mathbf{r}_I} \right|. \quad (3)$$

Although the magnifications of the individual images cannot be measured due to the small separations between the images, one can measure the

total magnification, i.e. $A = \sum_j^{N_I} A_j$, where N_I is the total number of images. Note that to find the image positions and the magnification, it is required to invert the lens equation.

For a single point-mass lens ($N = 1$), the lens equation can be easily inverted. Solving the equation yields two solutions of image positions and the total magnification is expressed in a simple analytical form of

$$A = \frac{u^2 + 2}{u\sqrt{u^2 + 4}}, \quad (4)$$

where $\mathbf{u} = (\mathbf{r}_S - \mathbf{r}_L)/\theta_E$ is the dimensionless lens-source separation vector normalized by θ_E . For a rectilinear lens-source transverse motion, the separation vector is related to the single lensing parameters by

$$\mathbf{u} = \left(\frac{t - t_0}{t_E} \right) \hat{\mathbf{x}} + \beta \hat{\mathbf{y}}, \quad (5)$$

where t_E represents the time required for the source to transit θ_E (Einstein time scale), β is the closest lens-source separation in units of θ_E (impact parameter), t_0 is the time of the maximum magnification, and the unit vectors $\hat{\mathbf{x}}$ and $\hat{\mathbf{y}}$ are parallel with and normal to the direction of the relative lens-source transverse motion, respectively. The light curve of a single point-mass lens event is characterized by its smooth and symmetric shape (Paczynski 1986).

If the lens system has additional components ($N \geq 2$), the lens equation cannot be algebraically inverted. However, the lens equation can be expressed as a polynomial in \mathbf{r}_I and the positions of the individual images are obtained by numerically solving the polynomial (Witt 1990). If the lens system is composed of two lenses (e.g. the primary and the planet), the lens equation is equivalent to a fifth-order polynomial in \mathbf{r}_I and there exist three or five solutions of the image positions depending on the source location with respect to the lens components. The main new feature of the multiple-lens system is the caustics, which represent the set of points in the source plane where the magnification of a point source becomes infinity, i.e. $|\det J| = 0$. Hence a significant planet-induced deviation in the lensing light curve occurs when the source approaches the region around the caustic although the duration of the deviation

is short due to the small mass ratio between the planet and the primary, q_p . The size of the caustic, and thus the probability of planet detections, also depends on the primary-planet separation and is maximized when the separation (normalized by θ_E) is in the range of $0.6 \lesssim d_p \lesssim 1.6$ (lensing zone).

As the number of lens components increases, solving the lens equation becomes nontrivial because the order of the polynomial increases by $N^2 + 1$. One other method commonly used to obtain the magnification patterns of multiple-lens systems is the inverse ray-shooting technique (Schneider & Weiss 1986; Kayser, Refsdal & Stabell 1986; Wambsganss 1997). In this method, a large number of light rays are uniformly shot backwards from the observer plane through the lens plane and then collected (binned) in the source plane. Then, the magnification pattern of the lens system is obtained by the ratio of the surface brightness (i.e., the number of rays per unit area) in the source plane to that in the observer plane. Once the magnification pattern is constructed, the light curve resulting from a particular source trajectory corresponds to the one-dimensional cut through the constructed magnification pattern. The advantage of using the ray-shooting method is that it allows one to study the lensing behavior regardless of the number of lens components. The disadvantage is that it requires a large computation time for the construction of the detailed magnification pattern. We attempted to investigate the lensing behaviors of multiple lens systems by solving the polynomial but we found that for the lens system of our interest for which the mass ratio between the least (satellite) and the most massive (primary) components is smaller than $\sim 10^{-5}$, the numerical noise in the polynomial coefficients due to the limited computer precision ($\sim 10^{-15}$) causes serious inaccuracy in solving the polynomial. We, therefore, use the ray-shooting method despite the requirement of large computation time.

3. Realistic Simulations

To examine the feasibility of detecting satellites of exoplanets, we carry out realistic simulations of Galactic bulge microlensing events caused by a lens system having a planet and a satellite. The primary of the tested lens system is assumed to

have a mass of $0.3 M_\odot$ by adopting that of a late-type main-sequence star, which is believed to be the most common type of lenses for events detected towards the Galactic bulge (Alcock et al. 2000). For the planet and the satellite, we test an Earth-mass planet and a Moon-mass satellite. Then, the mass ratios of the planet and the satellite with respect to the primary are $q_p = 10^{-5}$ and $q_s = 1.2 \times 10^{-7}$, respectively. The planet is assumed to be separated by $d_p = 1.3$ from the primary. To investigate the dependence of the magnification pattern on the satellite position with respect to the planet, we test four cases of satellite locations with different combinations of the planet-satellite separation, d_s (normalized by the Einstein ring radius of the planet $\theta_{E,p} = \sqrt{q_p} \theta_E$), and the orientation angle, α (measured from the primary-planet axis).

For a low-mass companion, the source size can have a significant effect on the shape of the companion-induced anomalies in lensing light curves (Bennett & Rhie 1996). For the construction of light curves, we, therefore, test three different types of source stars with angular radii of $\rho_\star = \theta_\star/\theta_E = 1.5 \times 10^{-3}$, 1.1×10^{-3} , and 0.85×10^{-3} . These values correspond to the source star radii of F0, G0, and K0 main-sequence stars located at $D_{OS} = 8.5$ kpc for an event with a lens located at the half way point between the observer and the source, i.e. $D_{OL}/D_{OS} = 0.5$. We note that although a M-type star has a smaller source radius ($\rho_\star = 0.6 \times 10^{-3}$ for M0 main sequence), we do not consider the case because the star will be too faint to be observed ($I \geq 25.6$ even without extinction). For comparison, we also present the light curves corresponding to a source with $\rho_\star = 3.0 \times 10^{-5}$, which is equivalent to the radius of a white dwarf. Although these events would be rare, there is at least some finite probability that a caustic crossing of a white dwarf would occur. In addition, although the brightness of a hot white dwarf would be faint ($V \gtrsim 25$), this is not much fainter than a typical K dwarf. Therefore, instead of presenting light curves of events involved with a hypothetical source star having an arbitrary radius, we present the light curves of events involved with a hot white dwarf.

In Figure 1, we present the magnification patterns (gray-scale maps in the right panels) around the regions of deviations induced by the planet

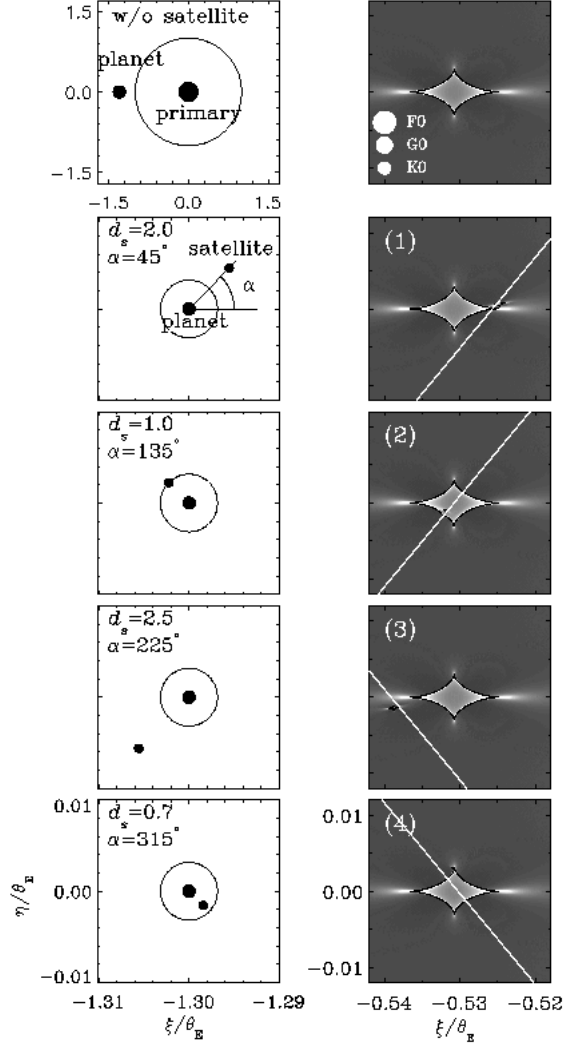


Fig. 1.— Magnification patterns of a lens system composed of a primary, a planet, and a subordinate satellite (gray-scale maps in the right panels) along with the corresponding geometries of the lens systems (left panels). For both the magnification maps and the lens system geometries, the coordinates are centered at the center of mass of the lens system and all lengths are normalized by θ_E . The circle in the upper left panel and those in the other left panels represent the Einstein rings of the primary and the planet (with a radius $\theta_{E,p} = \sqrt{q_p}\theta_E$), respectively. The planet is separated by $d_p = 1.3$ from the primary. The planet/primary and satellite/primary mass ratios are $q_p = 10^{-5}$ and $q_s = 1.2 \times 10^{-7}$, which correspond to a Earth-mass planet and a Moon-mass satellite around a $0.3M_\odot$ star, respectively. The labels in each of the left panel represent the planet-satellite separation, d_s (normalized by $\theta_{E,p}$), and the orientation angle, α (measured from the primary-planet axis). The solid curve in the magnification map represents the caustics. For comparison, we present the magnification pattern unperturbed by the satellite in the upper right panel. The three white dots in the upper right panel represent the source sizes (corresponding to those of F0, G0, and K0 main-sequence stars) which are used to construct the light curves in Fig. 2. The white lines in the right panels represent the source trajectories of the events, whose resulting light curves are presented in Fig. 2.

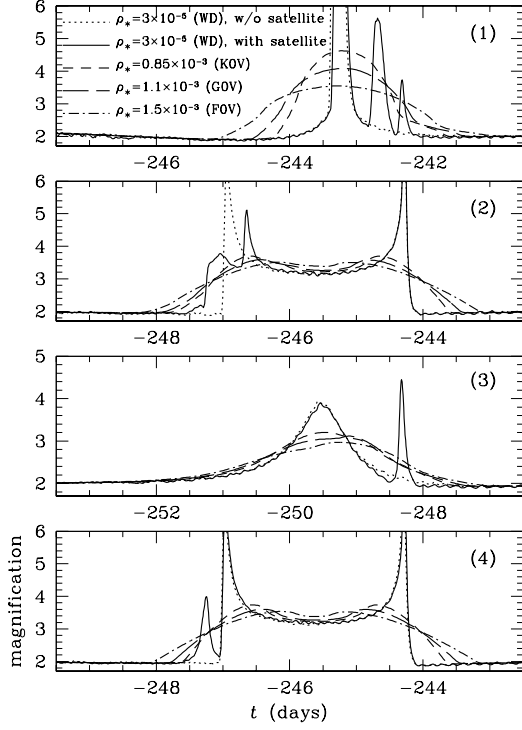


Fig. 2.— Variation of the lensing light curve anomalies induced by an Earth-mass planet having a Moon-mass satellite. In each panel, we present three different light curves involved with source stars having different angular radii of $\rho_* = \theta_*/\theta_E = 0.85 \times 10^{-3}$ (short-dashed curve), 1.1×10^{-3} (long-dashed curve), and 1.5×10^{-3} (dot-dashed curve), which correspond to the source radii of K0, G0, and F0 main-sequence stars for a Galactic bulge event caused by a lens with a total mass $m = 0.3M_\odot$ and located at $D_{OL}/D_{OS} = 0.5$. For comparison, we also present the light curves corresponding to the source of a white dwarf with $\rho_* = 3.0 \times 10^{-5}$, which are expected with (solid curve) and without the satellite (dotted curve). The source trajectories responsible for the light curves are marked on the magnification maps in Fig. 1, where the corresponding panels of the source trajectories and the light curves are marked by the same panel number. The time is presented in days assuming that the event has an Einstein timescale of $t_E = 30$ days. The reference of the time is arbitrarily set.

along with the corresponding geometries of the lens systems (left panels). In Figure 2, we also present the light curves of events resulting from the source trajectories marked in the corresponding panels in Fig. 1. From the simulations, we find the following results.

1. If the satellite is located within the lensing zone of the planet, i.e. $0.6 \lesssim d_s \lesssim 1.6^1$, the planet-induced caustic shape and the magnification pattern around the caustics are altered by the satellite due to the interference between the anomalies induced by the planet and the satellite [see panel (2) of Fig. 1].
2. If the satellite-planet separation is larger than the upper limit of the lensing zone of the planet, i.e. $d_s \gtrsim 1.6$, the interference becomes negligible. Then, the resulting magnification pattern is well represented by the superposition of those of the two binary systems where the planet-primary and the satellite-primary pairs act as independent lens systems (Bozza 1999; Han et al. 2001; Han & Park 2002; Rattenbury et al. 2002). Although the satellite is located beyond the planet's lensing zone, the satellite-planet separation is generally much smaller than the separation between the primary and the planet, i.e. $d_s \theta_{E,p} \ll d_p \theta_E$. Therefore, the additional deviations induced by the satellite is located near the region of planet-induced deviations.
3. If the satellite-planet separation is smaller than the lower limit of the lensing zone of the planet, i.e. $d_s \lesssim 0.6$, the planet-satellite pair behavior as if they are a single lens component with a mass equal to the combined one of the planet and the satellite. Since satellites are generally much less massive than their planets, i.e. $q_p + q_s \sim q_p$, and thus the lensing behavior in this case is hardly affected by the presence of the satellite.
4. The size (area) of the satellite-induced perturbation region is comparable or smaller

¹For a system of the Earth and the Moon located at $D_{OL}/D_{OS} \sim 0.5$, the Earth-Moon separation is about 3 times of the Einstein ring radius of an Earth-mass planet in the foreground of the Galactic bulge.

than the size of source stars that can be monitored from followup lensing observations. As a result, the detailed structure in the lensing light curves is seriously smeared out due to the finite source effect. We find that the finite source effect is so severe that the satellite signals in the light curves of all tested events are completely washed out even for events involved with K0 source stars.

4. Summary and Conclusion

We have tested the feasibility of detecting satellites by using microlensing. For this purpose, we have investigated the effect of satellites on the magnification pattern near the region of planet-induced perturbations by carrying out realistic simulations of Galactic bulge microlensing events. From this investigation, we find that although satellites can often affect the magnification patterns, detecting satellite signals in the lensing light curves will be very difficult because the signals are seriously smeared out by the severe finite source effect.

We would like to thank J. H. An for making useful comments about the work. This work was supported by a grant (2001-DS0074) from Korea Research Foundation (KRF).

REFERENCES

- Alcock C., et al., 2000, *ApJ*, 541, 734
- Bennett D. P., 2000, *BAAS*, 199, 115.05
- Bennett D. P., Rhie S. H., 1996, *ApJ*, 472, 660
- Bozza V., 1999, *A&A*, 348, 311
- Gould A., Loeb A., 1992, *ApJ*, 396, 104
- Han C., Chang H.-Y., An J. H., Chang K., 2001, *MNRAS*, 328, 986
- Han C., Park M.-G., 2002, *JKAS*, 35, 35
- Kayser R., Refsdal S., Stabell R., 1986, *A&A*, 166, 36
- Mao S., Paczyński B., 1991, *ApJ*, 374, L37
- Mayor M., Quozloz D., 1995, *Nature*, 37, 355
- Paczynski B., 1986, *ApJ*, 304, 1
- Perryman M. A. C., 2000, *Rep. Prog. Phys.*, 63, 1209
- Rattenbury N. J., Bond I. A., Skuljan J., Yock P. C. M., 2002, preprint (astro-ph/0204478)
- Sartoretti P., Schneider J., 1999, *A&AS*, 134, 553
- Schneider P., Weiss A., 1986, *A&A*, 164, 237
- Wambsganss J., 1997, *MNRAS*, 284, 172
- Witt H. J., 1990, *A&A*, 236, 311
- Wolszczan A., Frail D. A., 1992, *Nature*, 355, 145